PAPER

NJC
www.rsc.org/njc

Nucleation and growth of polyoxometalate nanoparticles in polyelectrolyte multilayer films

Yang Lan,[a] Enbo Wang,*[a] Yonghai Song,[b] Zhenhui Kang,[a] Lin Xu,[a] Zhuang Li[b] and Meiye Li[c]

[a] *Institute of Polyoxometalate Chemistry, Department of Chemistry, Northeast Normal University, Changchun, Jilin, 130024, P. R. China. E-mail: wangenbo@public.cc.jl.cn; Fax: +86-431-5684009; Tel: +86-431-5098787*

[b] *State Key Laboratory of Electroanalytical Chemistry, Changchun Institute of Applied Chemistry, Chinese Academy of Sciences, Jilin, 130022, P. R. China*

[c] *National Analytical Research Center of Electrochemistry and Spectroscopy Changchun Institute of Applied Chemistry, Chinese Academy of Sciences, Jilin, 130022, P. R. China*

Received (in Montpellier, France) 10th January 2005, Accepted 26th July 2005
First published as an Advance Article on the web 19th August 2005

An effective approach to the nucleation and growth of nanoparticles was performed for forming polyoxometalate based nanoparticles: $TBAB_3$–PMo_{12} (TBAB = tetrabutylammonium bromide, PMo_{12} = 12-molybdophosphoric anions) in multilayer films. The polyelectrolyte matrix was constructed by layer-by-layer self-assembly technology. The nucleation and growth of PMo_{12} nanoparticles was achieved by alternately dipping the precursor films into PMo_{12} and TBAB solutions, in which TBAB was employed as precipitator. Repeating the above process of absorption and precipitation of PMo_{12} anions, the PMo_{12} nanoparticles were of controllable synthesis in the multilayer films. The variation of the size and morphology of PMo_{12} nanoparticles was accomplished by increasing adsorption and precipitation cycle number, which was detected by transmission electron microscopy and scanning electron microscopy. The growth process, composition, and surface topography of the multilayer films containing PMo_{12} nanoparticles were investigated by UV–Vis spectroscopy, Fourier transform infrared (FTIR) spectroscopy, and atomic force microscopy (AFM). The electrochemical properties were studied through cyclic voltammograms when the substrate was indium–tin oxide and the films presented good stability and similar electrochemical behavior to that of PMo_{12} in aqueous solution.

Introduction

Advanced materials composed of nano-sized particles hold substantial promise for potential applications in some technological areas. In particular, nanoparticles in polymer matrixes arouse interest, since they have been commonly used as thin films in optical, electrical, and magnetic devices.[1] Several methods were applied to synthesize such films such as casting, spraying, sol–gel and so on. To date it is still a challenge to choose a good approach for the controllable synthesis and growth of nanoparticles in thin films so as to specify the size, surface morphology and hence their properties.[2] Layer-by-layer (LbL) self-assembly technology based on alternating adsorption provides a convenient method for thin film deposition.[3] This method has been widely employed for the formation of multilayer films of a wide variety of materials such as proteins,[4] DNA,[5] dendrimers,[6] inorganic species[7] and so on. Recently, LbL technology has been extensively applied to construct polyelectrolyte and nanoparticle composite films.[2a,8] The charged nanoparticles can be directly incorporated into the polyelectrolyte multilayer films by this means, but they are liable to aggregate and cannot disperse well in the films. However, the *in situ* synthesis method avoids the above problem, since the nanoparticles can be selectively and controllably defined in specific areas of the polyelectrolyte films. It is noteworthy that there are two ways to realize *in situ* synthesis of nanoparticles in polyelectrolyte multilayer films. One is to form nanoparticle-containing films by sequential adsorption of positively charged polyelectrolyte and negatively charged polyelectrolyte with metal ions in either, and then, post-deposition of the metal ions by means of reduction, sulfidation or hydrolysis and so on.[9] The other method is nucleation and growth of the nanoparticles in multilayer films, which was described by Stroeve's group.[10] This method produces precursor polyelectrolyte multilayer films *via* LbL and then nucleation of nanoparticles was initiated by adsorption and hydrolysis of small metal ions. By repeating the adsorption and hydrolysis process, the nanoparticles grow gradually in the dimension of the crystallites. Both of these two methods can make nanoparticles disperse well, and thus control the thickness of multilayer films and the size of nanoparticles. However, it is interesting that the latter can control the morphology of nanoparticles, and consequently give nano- or microcrystals by increasing the cycle numbers of adsorption and hydrolysis.

Polyoxometalates (POMs) having enormous variation in topology, size, electronic properties and elemental composition present a class of unique inorganic entities, which have been extensively studied in catalysis, materials chemistry, biochemistry and so on.[11] They can be regarded as one of the potential candidates to be transformed into nanometre-sized materials. It is believed that the preparation of nano-sized POMs can provide a new route for exhibiting their unique properties in many fields. Recently, POM nanoparticles and nanocrystals have been successfully prepared.[12] Moreover, POM nanoparticles have been controllably synthesized in polyelectrolyte

DOI: 10.1039/b500293a

multilayer films *via* LbL technology, which made use of the former type of *in situ* synthesis.[13]

In this article, the multilayer films containing POM nanoparticles were prepared by utilizing the later type of *in situ* synthesis provided by Stroeve. 12-Molybdophosphoric anions (PMo_{12}) were used instead of small metal ions and tetrabutylammonium bromide (TBAB) was employed as precipitator to combine with PMo_{12} in order to achieve the nucleation and growth of nanoparticles. The size of the POM nanoparticles increased and the morphology of them changed from spherical to egg-shaped on the increase of adsorption and precipitation. Furthermore, the electrochemistry of the multilayer films containing PMo_{12} nanoparticles was studied. They showed good stability in electrochemistry experiments and retained the electrochemical activity of PMo_{12}.

Experimental

Reagents

Poly(diallyldimethylammonium chloride) (PDDA, MW $\approx$ 100 000–2000 000) and poly(styrenesulfonate) sodium salt (PSS, MW $\approx$ 70 000) were purchased from Aldrich and used as received. Polyoxometalates with the composition $H_3PMo_{12}O_{40}$ (PMo_{12}) and $H_4SiW_{12}O_{40}\cdot nH_2O$ (SiW_{12}) were prepared according to the literature procedure.[14] All of the other chemicals are of reagent grade.

Instruments

UV–Vis absorption spectra were recorded on a quartz slide using a 752 PC UV–Vis spectrophotometer. The FTIR absorption spectra were obtained in absorbance mode using a Bio-Rad FTS135 spectrophotometer on silicon wafers. TEM measurements were carried out on a Hitachi H-600 microscope to collect the morphology of the POMs nanoparticles in films. AFM images were taken on mica under a Digital Instruments Nanoscope IIIa instrument operating in tapping mode with silicon nitride tips under ambient conditions. SEM measurements were performed on an XL30 ESEM FEG scanning electron microscope (FEI Company) operating at an accelerating voltage of 30 kV. The electrochemical experiments were performed on a CHI 660 electrochemical workstation connected to a digital-586 personal computer by using a conventional three-electrode system. A saturated calomel electrode (SCE) was used as the reference electrode, Pt gauze as a counter electrode, and ITO as a working electrode.

Multilayer assembly

PDDA–PSS multilayer films were fabricated on quartz slides, mica, or silicon wafers. The quartz slides or silicon wafers were cleaned by ultrasonication in Piranha solution (H_2O_2–H_2SO_4 3 : 7 v/v) for 30 min prior to deposition. Then, the substrates were washed thoroughly with doubly deionized water and further purified by immersing in NH_4OH–H_2O_2–H_2O (1 : 1 : 5 v/v) solution at 70 °C for 30 min, followed by rinsing with plenty of doubly deionized water and drying with nitrogen. The substrate was completely hydrophilic after the above two cleaning approaches. Polyelectrolyte multilayer films were obtained by alternately depositing PDDA (20 mM) and PSS (1 mg mL^{-1}) on the cleaned quartz slide for 20 min, respectively. Deionized water and HCl solution (pH = 4.5) were used for rinsing after each immersion step. The polycation monolayer together with that of polyanions is called a bilayer. When the desired number of bilayers was achieved, the substrate was dipped into POM (POM = PMo_{12} or SiW_{12}) (0.02 mol L^{-1}) and tetrabutylammonium bromide (TBAB) (0.02 mol L^{-1}) aqueous solution for 1 min and 2 min, respectively. Rinsing and immersing with deionized water and drying with N_2 were performed after each deposition step. This process was called one adsorption and precipitation cycle and was repeated after 20 min. The above procedure results in the build-up of multilayer films containing POM nanoparticles, which can be expressed as $(PDDA–PSS)_n$–$[(TBAB)_xPOM]_m$, where n is the number of bilayers and m is the number of cycles of adsorption and precipitation (POM = PMo_{12}, $x = 3$; POMs = SiW_{12}, $x = 4$).

Results and discussion

The growth process of multilayer films containing POMs nanoparticles was investigated by means of UV–Vis spectra. Fig. 1a shows the UV–Vis spectra of $(PDDA–PSS)_{5.5}$–$(TBAB_3–PMo_{12})_n$ multilayer films with n from 0 to 8. Since PDDA does not absorb above 200 nm, the absorption band at 225 nm is due to the aromatic group of PSS molecules in the pristine film with $n = 0$. With the adsorption and precipitation cycle number n increasing (from 1 to 8), it is amazing that the absorption band at 225 nm gradually became weaker while the peaks at 219 nm and 311 nm were stronger and stronger. These two peaks at 219 and 311 nm are the characteristic bands of PMo_{12} corresponding to the O → Mo charge transfer transition. Further-

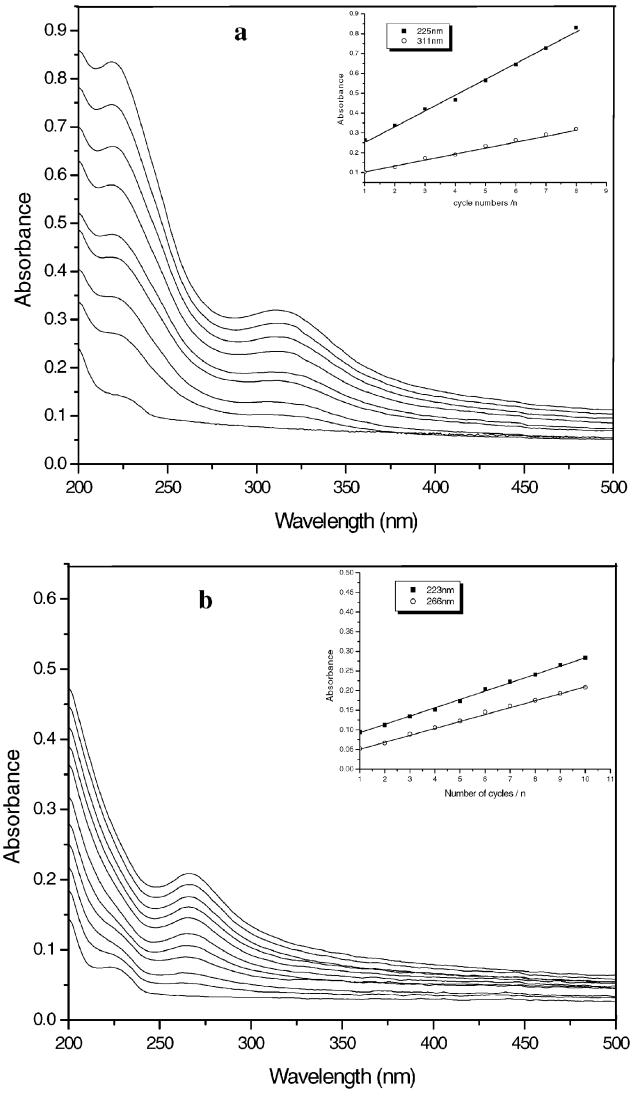

Fig. 1 (a) UV–Vis spectra of $(PDDA–PSS)_{5.5}$–$(TBAB_3–PMo_{12})_n$ films with $n = 0$–8 on quartz substrates. The inset shows the plots of the absorbance values at 222 nm, 311 nm *versus* the number of precipitation cycles. (b) for $(PDDA–PSS)_{5.5}$–$(TBAB_4–SiW_{12})_n$ films with $n =$ 0–10. Inset: absorbance at 223 nm, 266 nm *versus* the number of precipitation cycles.

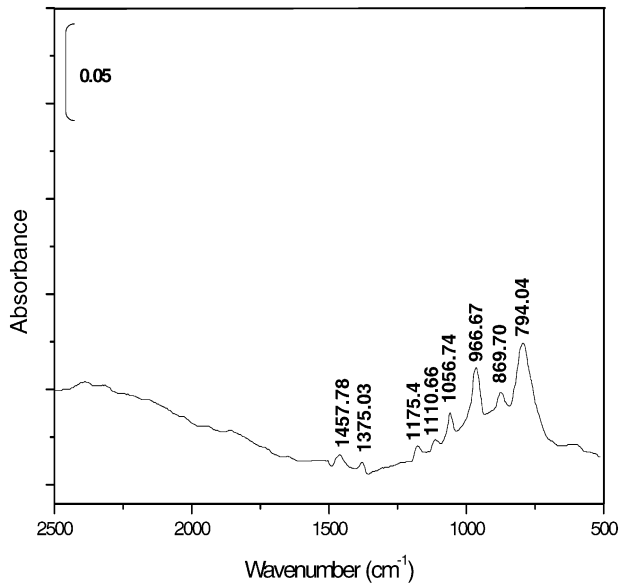

Fig. 2 FTIR spectrum of PDDA–PSS polyelectrolyte multilayer films containing $TBAB_3$–PMo_{12} nanoparticles absorbed on the silicon wafer.

more they are red shifted (216 nm to 219 nm, 306 to 311 nm) as n changes from 1 to 8, which indicates that PMo_{12} combined with TBAB to form stable nanoparticles and their size increased with increasing cycle number n. But it is not certain whether or not the peak at 225 nm has disappeared, since it is so close to the peak at 219 nm. In the following experiment, the SiW_{12} having no absorption peak between 210 nm and 250 nm was chosen to integrate with TBAB to form nanoparticles in the films. The formation of multilayer films with the composition $(PDDA–PSS)_{5.5}$–$(TBAB_4–SiW_{12})_n$ (n from 0 to 14) was also detected by UV–Vis (See Fig. 1b). From the figure, the characteristic bond of SiW_{12} at 266 nm is due to the oxygen to tungsten charge transfer transition, which suggested the incorporation of SiW_{12} into multilayer films. It is also clear that the characteristic peak of PSS at 223 nm becomes weaker and weaker until it disappears with increasing deposition cycle number n. This indicates the loss of PSS in the formation process of POM nanoparticles. But as we know, PDDA and PSS are strong polyelectrolytes and the electrostatic interaction between these two compositions in the films is not labile to acid or base, so the multilayer films should be stable when they were exposed to acidic or alkaline solution. Moreover, plotting the absorbance of multilayer films containing POM nanoparticles at the characteristic wavelengths of PSS and POMs *versus* precipitation cycle n results in nearly straight lines (see insets in Fig 1a. and Fig 1b). This linear increase confirms that the process of adsorption of POMs in the films and the subsequent precipitation with TBAB is a reproducible process, although the adsorption peak of PSS eventually disappeared. That is to say the films are not prone to the loss of PSS, since the POMs were chosen to form nanoparticles in the film. POMs as a kind of special charged cluster can be incorporated into polyelectrolyte multilayer films and are not liable to leach out,[15] which is different from low molecular weight species such as multi-charged metal ions and molecular dyes.[2b] Although the reason why PSS was absent when the POMs were incorporated into the multilayer films is not very clear, it may be related to the existence of POMs affecting the composition of the formed PDDA–PSS multilayer films according to a study on blended thin films.[16]

FTIR spectroscopy was used to measure the composition of films. Fig. 2 represents the FTIR spectra of polyelectrolyte multilayer films containing $TBAB_3$–PMo_{12} nanoparticles. The FTIR spectrum has regions as follows: the absorption bands at 1056.74, 966.67, 869.70, and 794.04 cm^{-1} are the characteristic bands of PMo_{12}, which should be ascribed to the vibration

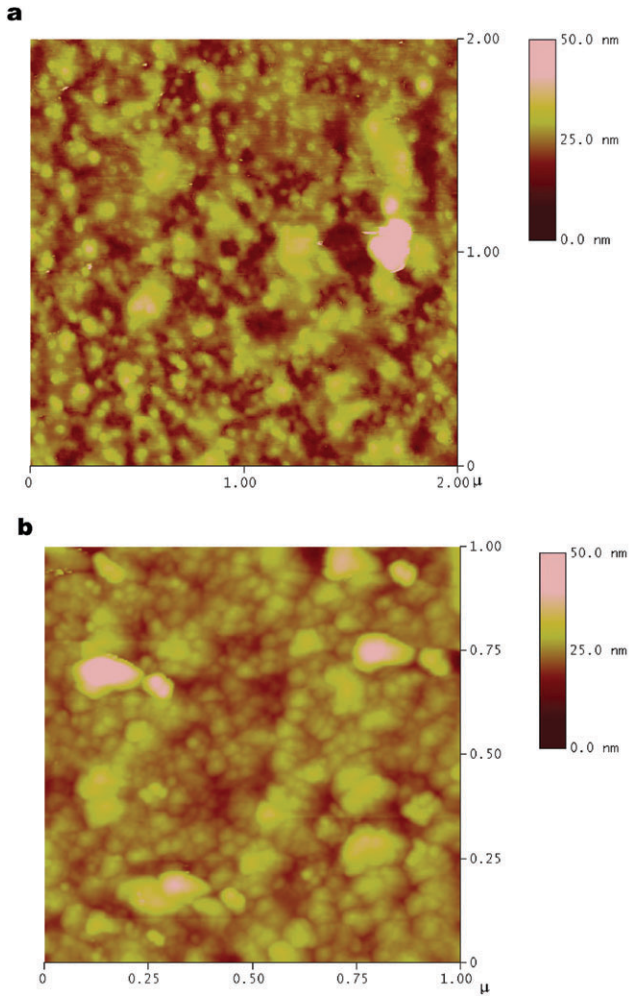

Fig. 3 Tapping mode AFM image of $(PDDA–PSS)_{3.5}$–$(TBAB_3–PMo_{12})_2$ multilayer films on mica: (a) $[PMo_{12}] = 0.02$ mol L^{-1}; (b) $[PMo_{12}] = 0.04$ mol L^{-1}.

modes of ν (P═O_a†), ν (Mo═O_t), ν (Mo–O_b–Mo) and (Mo–O_c–Mo), respectively. Furthermore, the multilayer films also exhibit vibration bands at 1100 to 1500 cm^{-1} (νC–H, νC–N) due to the PDDA and TBAB components. It should be noted that the characteristic bands of PSS are absent in the FTIR spectrum; the characteristic bands should appear around 1171, 1123, 1035, and 1008 cm^{-1}. These results indicate that PMo_{12} has been produced in the multilayer films and the basic structure of PMo_{12} is preserved while the PSS of the precursor polyelectrolyte films disappeared, supporting the results from the UV–Vis spectra.

The information concerning the surface morphology variation of the $(PDDA–PSS)_{3.5}$ multilayer films alternately exposed to PMo_{12} solution and TBAB solution with different concentrations of PMo_{12} was explored using AFM in tapping mode (See Fig. 3). Fig. 3a shows the image of the state of the polyelectrolyte pristine films after carrying out two cycles of adsorption and precipitation when the concentration of PMo_{12} was 0.02 mol L^{-1}, and Fig. 3b is for the films obtained after two cycles with a concentration of 0.04 mol L^{-1}. As can be seen from Fig. 3a, the composite film surface is made up of many spherical domains and some irregular blocks. The diameters of the spherical domains are from 20 nm to 70 nm along the horizontal axis. These domains are attributed to the formation of $TBAB_3$–PMo_{12} nanoparticles. The nanoparticles are closely packed with each other, forming a uniform surface with the

† O_a, oxygen in P–O tetrahedron; O_t, terminal oxygens; O_b, bridging OM_2 oxygens; O_c, central OM_6.

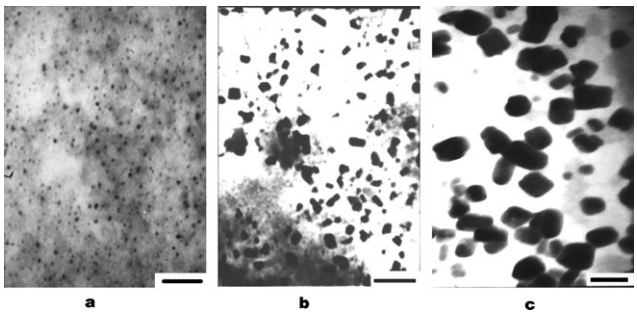

Fig. 4 TEM micrographs of 5.5-bilayer films of PDDA and PSS after different n cycles of adsorption and precipitation of PMo_{12} (a) $n = 2$, bar size = 250 nm; (b) $n = 6$, bar size= 333 nm; (c) $n = 12$, bar size = 333 nm.

polyelectrolyte. The irregular blocks may be due to the fact that POM nanoparticles have grown up based on the initial nanoparticles. From Fig. 3b it can be seen that the quantity of the domains increases and most of the domains appear irregular and nub-like. That is to say, there are more nanoparticles formed as the concentration of PMo_{12} increased and they have grown up based on other initial nanoparticles.

TEM is a convenient method to examine the finest details of the internal structure of micro- and nano-scale matter. The variation of a 5.5 bilayer of PDDA–PSS film in the process of POMs (PMo_{12}) nanoparticle formation was explored using TEM (see Fig. 4a–4c). Fig. 4a shows the micrograph corresponding to the initial forming stages of POM nanoparticles with adsorption and precipitation cycle number $n = 2$ and the concentration of PMo_{12} is 0.02 mol L^{-1}. The spherical POM nanoparticles are well dispersed in the film matrix with sizes from 20 to 60 nm. It can be seen that the nanoparticles are not completely spherical but some of them appeared irregular and nub-like. This was also highlighted in the AFM study of the films, and could be due to the nanoparticles growing on the initial ones in lateral expansion mode.[2a] Increasing the adsorption and precipitation cycle number ($n = 6$) results in an increase in the size of the $TBAB_3$–PMo_{12} nanoparticles and their morphology is nub-like and club-like (see Fig 4b). Continuing to increase the number of absorption–precipitation cycles n to 12, larger POM nanoparticles of egg-shape were obtained (see Fig. 4c). Moreover, it also can be seen that there is a small quantity of spherical nanoparticles in the films besides the large ones formed in Fig. 4b and Fig. 4c, which indicates the formation of small $TBAB_3$–PMo_{12} nanoparticles at this stage of their growth process.[9c] From Fig. 4, it can be concluded that not only the size of the $TBAB_3$–PMo_{12} nanoparticles increased but also their morphology is changed continuously with the increase in cycle number. The initially formed PMo_{12} nanoparticles can be regarded as the core for the subsequent growth of the nanoparticles on them in the dimension of the crystallites (non-spherical), but nano-crystallites of $TBAB_3$–PMo_{12} were not obtained as expected. The possible reasons may be that the long chains of TBAB as counterions and the rapid precipitation of POMs and TBAB prevented them from forming an ordered crystalline structure. The study of the preparation of the nano-crystallites of PMo_{12} through the nucleation and growth method herein is under way.

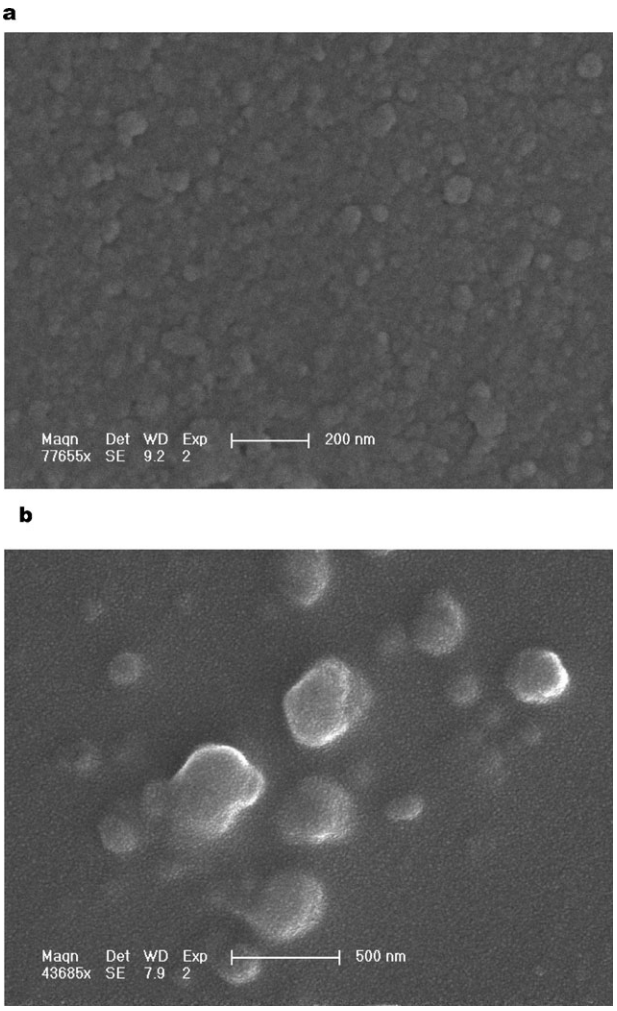

Fig. 5 SEM images of the 5.5-bilayer polyelectrolyte films after n cycles of assembly (a) $n = 2$; (b) $n = 12$.

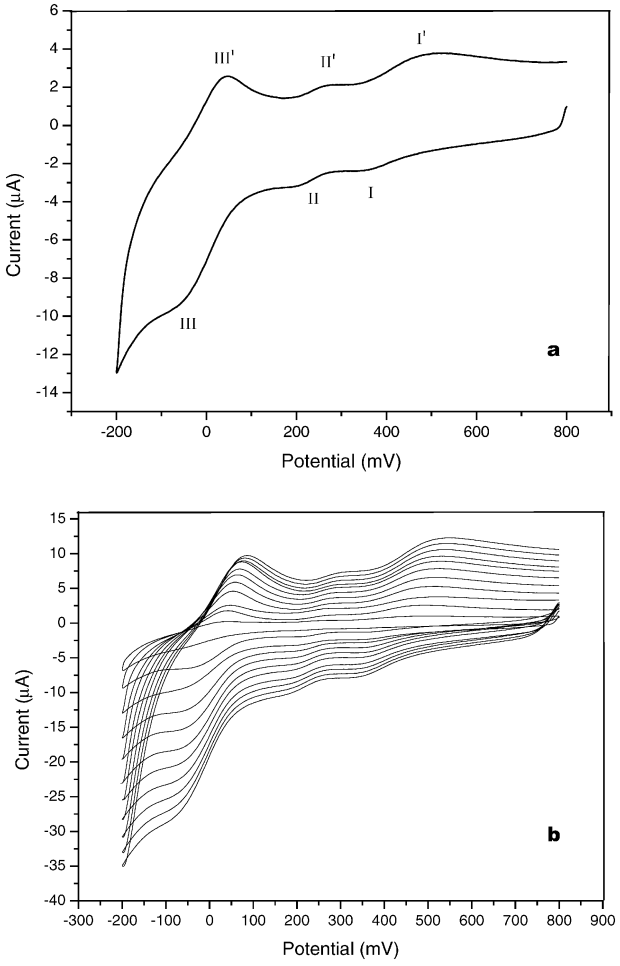

Fig. 6 Cyclic voltammograms of $(PDDA–PSS)_{5.5}$–$(TBAB_3–PMo_{12})_6$ films on ITO electrode in 1M H_2SO_4 solution (a) at 50 mV s^{-1} and (b) at different scan rates (from inner to outer: 20, 40, 50, 60, 80, 100, 120, 140, 160, 180, 200 mV s^{-1}). Potentials *vs.* SCE.

Fig. 5 presents top view SEM images of the multilayer films after different adsorption and precipitation cycle numbers (Fig. 5a is for $n = 2$ and Fig. 5b is for $n = 12$) assembled on a silicon wafer. These two SEM profiles demonstrate an obvious increase in size of the nanoparticles with increasing number of assembly cycle. The surface of the multilayer films is relatively smooth with the nanoparticles embedded in it, and its size is around 50 nm and 200 nm along the horizontal axis, respectively.

In our previous work, an inorganic–organic hybrid POM nanoparticle modified wax-impregnated graphite electrode and carbon paste electrode were prepared,[17] while an electrode modified with ultra thin films containing inorganic–organic POM nanoparticles has not till now been reported. The electrochemical properties of the multilayer films containing $TBAB_3$–PMo_{12} nanoparticles were studied when the substrate was ITO. The ITO was immersed in a saturated sodium methanol solution for 2 days to form a hydrophilic surface before LbL assembly. Fig. 6a shows the cyclic voltammograms (CVs) of the films $(PDDA–PSS)_{5.5}$–$(TBAB_3–PMo_{12})_6$ in 1 M H_2SO_4 aqueous solutions. In the potential range from +800 to −200 mV, three reversible redox peaks appeared and the mean peak potentials $E_{1/2} = (E_{pa} + E_{pc})/2$ are 424(I), 239(II), 6(III) mV, respectively. The three redox peaks correspond to three consecutive two-electron processes.[17a] Fig. 6b is the CVs of the multilayer films containing $TBAB_3$–PMo_{12} nanoparticles at different scan rates in 1 M H_2SO_4. When the scan rates changed from 10 to 200 mV s^{-1}, the peak current increased gradually and the cathodic peak potentials shifted to the negative direction and the corresponding anodic peak potentials shifted to the positive direction. These results show that the films containing $TBAB_3$–PMo_{12} nanoparticles present similar electrochemical behavior to that of PMo_{12} in aqueous solution.[18] Moreover, the films exhibited good stability due to the insolubility of PMo_{12}–TBAB nanoparticles in the electrochemistry experiment. When the potential range is maintained from −200 to 800 mV, the current response of the films remained almost unchanged even after 100 scan cycles at a rate of 50 mV s^{-1}. That is to say multilayer films containing POM nanoparticles display stable electrochemical properties. To date, few of the POM–polyelectrolyte multilayer films constructed *via* electrostatic LbL assembly represent this kind of electrochemistry stability because of the solubility of POMs.[19]

Conclusions

In this article, controllable synthesis of $TBAB_3$–PMo_{12} nanoparticles in polyelectrolyte multilayer films was presented using the *in situ* nucleation and growth method. The LbL self-assembly technique was used to form precursor films for adsorption and precipitation of PMo_{12} and then detailed characterization of nucleation and growth of PMo_{12} nanoparticles was performed. The adsorbed PMo_{12} polyanions were attached to positively charged PDDA in the films for the formation of nanoparticles and simultaneously substituted passively charged PSS of the precursor films. The growth of nanoparticles is a reproducible process and the structure of the films was not damaged according to the study of UV–Vis characterization. The size and morphology of PMo_{12} nanoparticles can be controlled by increasing the adsorption and precipitation cycle numbers. Moreover, PMo_{12} nanoparticle-based polyelectrolyte films exhibit good stability and electrochemical properties similar to that of PMo_{12} in aqueous solution. Finally it is believed that the nucleation and growth approach can be applied to synthesize other categories of POMs nanoparticles. The results obtained herein may broaden the applications field of POM nanoparticles in catalysis and electrical devices.

Acknowledgements

This work was financially supported by the National Natural Science Foundation of China (20371011).

References

1 (*a*) Z. Y. Tang, N. A. Kotov and M. Giersig, *Science*, 2002, **297**, 237; (*b*) W. C. W. Chan and S. M. Nie, *Science*, 1998, **281**, 2016; (*c*) S. J. Park, T. A. Taton and C. A. Mirkin, *Science*, 2002, **295**, 1503.
2 (*a*) J. W. Ostrander, A. A. Mamedov and N. A. Kotov, *J. Am. Chem. Soc.*, 2001, **123**, 1101; (*b*) N. A. Kotov, in *Multilayer Thin Films—Sequential Assembly of Nanocomposite Materials, P208*, ed. G. Decher and J. B. Schlenoff, Wiley-VCH, Weinheim, 2003.
3 (*a*) G. Decher, *Science*, 1997, **277**, 1232; (*b*) X. Zhang and J. C. Shen, *Adv. Mater.*, 1999, **11**, 1139.
4 Y. Lvov, Z. Lu, J. B. Schenkman, X. Zu and J. F. Rusling, *J. Am. Chem. Soc.*, 1998, **120**, 4073.
5 S. Jiang and M. Liu, *J. Phys. Chem. B*, 2004, **108**, 2880.
6 (*a*) H. Y. Zhang, Y. Fu, D. Wang, L. Y. Wang, Z. Q. Wang and X. Zhang, *Langmuir*, 2003, **19**, 8497; (*b*) H. Y. Zhang, Z. Q. Wang, Y. Q. Zhang and X. Zhang, *Langmuir*, 2004, **20**, 9366.
7 S. Q. Liu, D. G. Kurth, B. Bredenkötter and D. Volkmer, *J. Am. Chem. Soc.*, 2002, **124**, 12279.
8 T. Cassagneau, T. E. Mallouk and J. H. Fendler, *J. Am. Chem. Soc.*, 1998, **120**, 7848.
9 (*a*) T. C. Wang, M. F. Rubner and R. E. Cohen, *Chem. Mater.*, 2003, **15**, 299; (*b*) J. H. Dai and M. L. Bruening, *Nano Lett.*, 2002, **2**, 497; (*c*) T. C. Wang, M. F. Rubner and R. E. Cohen, *Langmuir*, 2002, **18**, 3370; (*d*) S. Joly, R. Kane, L. Radzilowski, T. Wang, A. Wu, R. E. Cohen, E. L. Thomas and M. F. Rubner, *Langmuir*, 2000, **16**, 1354.
10 (*a*) S. Dante, Z. Z. Hou, S. Risbud and P. Stroeve, *Langmuir*, 1999, **15**, 2176; (*b*) L. Q. Zhang, A. K. Dutta, G. Jarero and P. Stroeve, *Langmuir*, 2000, **16**, 7095; (*c*) A. K. Dutta, G. Jarero, L. Q. Zhang and P. Stroeve, *Chem. Mater.*, 2000, **12**, 176; (*d*) A. K. Dutta, T. Ho, L. Q. Zhang and P. Stroeve, *Chem. Mater.*, 2000, **12**, 1042; (*e*) A. M. Fojas, E. Murphy and P. Stroeve, *Ind. Eng. Chem. Res.*, 2002, **41**, 2662; (*f*) P. Stroeve, *Nucleation of Nanoparticles in Ultrathin Polymer Films in Encyclopedia of Nanoscience Nanotechnology*, Marcel Dekker, New York, 2004, pp. 2713–2719.
11 (*a*) M. T. Pope and A. Müller, *Angew. Chem., Int. Ed. Engl.*, 1991, **30**, 34–48; (*b*) R. J. Errington, in *Polyoxometalate Chemistry from Topology via Self-assembly to Applications*, ed. M. T. Pope and A. Müller, Kluwer, Netherlands, 2001, pp. 7–22; (*c*) A. Müller, Y. S. Zhou, L. J. Zhang, H. Bögge, M. Schmidtmann, M. Dresselb and J. V. Slagerenb, *Chem. Commun.*, 2004, 2038.
12 (*a*) T. Ito, K. Inumaru and M. Misono, *Chem. Mater.*, 2001, **13**, 824; (*b*) Z. H. Kang, E. B. Wang, M. Jiang and S. Y. Lian, *Eur. J. Inorg. Chem.*, 2003, **2**, 370.
13 M. Jiang, E. B. Wang, Z. H. Kang, S. Y. Lian, A. G. Wu and Z. Li, *J. Mater. Chem.*, 2003, **13**, 647.
14 M. Filowitz, R. K. C. Ho, W. G. Klemperer and W. Shum, *Inorg. Chem.*, 1979, **18**, 93, and references therein.
15 (*a*) D. G. Kurth, D. Volkmer, M. Ruttorf, B. Richter and A. Müller, *Chem. Mater.*, 2000, **12**, 2829; (*b*) S. Q. Liu, D. Volkmer and D. G. Kurth, *J. Cluster Sci.*, 2003, **14**, 405; (*c*) M. Jiang, E. B. Wang, G. Wei, L. Xu, Z. H. Kang and Z. Li, *New J. Chem.*, 2003, **27**, 1291.
16 (*a*) J. Cho, J. F. Quinn and F. Caruso, *J. Am. Chem. Soc.*, 2004, **126**, 2270; (*b*) J. F. Quinn, J. C. C. Yeo and F. Caruso, *Macromolecules*, 2004, **37**, 6537.
17 (*a*) X. L. Wang, Z. H. Kang, E. B. Wang and C. W. Hu, *J. Electroanal. Chem.*, 2002, **523**, 142; (*b*) X. L. Wang, E. B. Wang, Y. Lan and C. W. Hu, *Electroanalysis*, 2002, **14**, 1116.
18 K. Unoura and N. Tanaka, *Inorg. Chem.*, 1983, **22**, 2963.
19 S. Q. Liu, Z. Y. Tang, Z. X. Wang, Z. Q. Peng, E. K. Wang and S. J. Dong, *J. Mater. Chem.*, 2000, **10**, 2727.